PAPER

Check for updates

Simple fluorochromic detection of chromium with ascorbic acid functionalized luminescent Bio-MOF-1†

Gurjeet Kaur,[a,b] Saloni Sharma,[a,b] Neha Bhardwaj, [iD][c] Manoj K. Nayak [iD] *[a,b] and Akash Deep [iD] *[a,c]

The bioaccumulation of various heavy metals in the environment and agriculture is posing serious hazards to human health. Hexavalent chromium is one of the most encountered heavy metal pollutants. The routine monitoring of Cr(VI) *via* simple methods assumes great analytical significance in sectors like environmental safety, food quality, *etc*. This study reports a novel biocompatible and luminescent metal–organic framework (ascorbic acid functionalized Bio-MOF-1) based "Turn-on" nanoprobe for rapid and sensitive optical detection of Cr(VI). Bio-MOF-1 has been synthesized, functionalized with ascorbic acid (AA), and then comprehensively characterized for its key material properties. The presence of Cr(VI) results in the photoluminescence recovery of Bio-MOF-1/AA. Using the above approach, Cr(VI) is detected over a wide concentration range of 0.02 to 20 ng mL^{-1}, with the limit of detection being 0.01 ng mL^{-1}. The nanoprobe is capable of detecting Cr(VI) in real water as well as in some spiked food samples. Hence, the ascorbic acid functionalized Bio-MOF-1 nanoprobe is established as a potential on-field detection tool for Cr(VI).

1. Introduction

Chromium and its compounds are extensively distributed in the environment. Amongst different forms, Cr(III) has been recognized as an essential element in maintaining lipid and protein metabolism.[1] Its deficiency in the human body may cause health disorders, such as diabetes mellitus, myopathy in children, and hypoglycemia.[2] The metal and chemical industries, like tanning and pigments, steel, nonferrous alloys, *etc.*, are the leading anthropogenic sources of chromium. Under certain natural conditions, Cr(III) is oxidized to Cr(VI) which is known for its carcinogenic properties and other toxic effects on biological systems.[3] Globally, hexavalent chromium is recognized as one of the most concerning toxic heavy metals that are harmful to humans as well as the ecosystem.[4–6] Cr(VI) not only contaminates the water bodies, but also penetrates into the soil to ultimately accumulate within plants. Hence, concerns have been raised about the entry of Cr(VI) into the food chain and its percolation in the human system, affecting

the kidneys, gastrointestinal tract, respiratory tract, liver, *etc.*[7–10] Since 1982, the International Agency for Research on Cancer (IARC) has classified Cr(VI) as a potent carcinogen because of its ability to modify DNA transcription processes to cause chromosomal abnormalities.[11] As per USEPA, 0.1 milligrams per litre (or 100 parts per billion) is the maximum permissible concentration of Cr(VI) in drinking water.[12–14]

In general, metal concentrations are determined with techniques like atomic absorption spectrometry,[15] inductively coupled plasma-mass spectrometry,[16] flame atomic absorption spectrometry,[17] X-ray fluorescence analysis, chromatographic analyses, chemiluminescence methods, and high-performance liquid chromatography.[18] Nonetheless, there is a great demand to develop methods that allow low-cost, portable, routine, rapid, and easy-to-deploy detection of heavy metals so that a more routine screening of environmental and food samples can be guaranteed. In this context, chemosensors assume a great analytical significance. The application of advanced nanomaterials, such as quantum dots, nanoparticles, and synthetic fluorophores, has greatly contributed towards the development of efficient chemosensors for diverse analytes, including heavy metals such as Hg(II)[19,20] and Cr(VI).[21–25] In particular, nanomaterial-based fluorescence chemosensors are generally known for their portability, high surface-to-volume ratios, amplified output response, strong surface reactivity, and good chemical/thermal stability.[26,27]

Most of the optical chemosensors reported for Cr(VI) are based on the fluorescence quenching or fluorescence recovery

[a]Academy of Scientific and Innovative Research (AcSIR), Ghaziabad-201002, Uttar Pradesh, India
[b]CSIR-Central Scientific Instruments Organization (CSIR-CSIO), Sector 30C, Chandigarh-160030, India. E-mail: mknayak@csio.res.in
[c]Institute of Nano Science and Technology (INST), Sector 81, S.A.S. Nagar (Mohali), Punjab-140306, India. E-mail: akashdeep@inst.ac.in
†Electronic supplementary information (ESI) available. See DOI: https://doi.org/10.1039/d4nr00768a

mechanisms. For instance, Duan *et al.* developed a fluorescence sensor for Cr(VI) using the g-C$_3$N$_4$/Fe$_3$O$_4$ nanocomposite, which possessed good fluorescence and magnetic properties.[28] This sensor offered a limit of detection (LOD) of 0.5 μM. A fluorescent nanocomposite of doped polyaniline, 2-acrylamido-2-methylpropanesulfonic acid capped Ag nanoparticles and graphene oxide quantum dots has been reported to selectively detect Cr(VI) ions in the range from 0.01 to 7.5 mg L^{-1} with a LOD of 6 μg L^{-1}.[29] Bilgic *et al.* proposed super paramagnetic fluorescence nanoparticles (F-SPION) for the detection of Cr(VI).[30] Similarly, many Schiff bases have also been reported in the literature for the fluorescence detection of Cr(VI).[31–34] Nanogold-functionalized poly(amidoamine) has been decorated with enzyme-tyramine concatemers and used for the detection of Hg^{2+} ions with a low LOD of 0.4 pM.[35] A fluorometric bioanalysis sensing system for Hg^{2+} was developed using ultrathin 2-D MXenes as fluorescence quenchers in a probe containing Hg^{2+} induced exonuclease III (Exo-III). This Exo-III-assisted target recycling method allowed efficient signal amplification and facilitated an LOD of 42.5 pM.[20]

Metal–organic frameworks (MOFs) endowed with fascinating optical properties and structural diversity have emerged as highly useful materials for developing various types of optical chemosensors for analytes, such as emerging contaminants, food-borne pathogens, biomarkers, *etc.*[36–38] Compared to other fluorophores, luminescent MOFs are characterized by certain superior material properties as they possess features like high surface areas, crystallinity, stable fluorescence, accessible pores to facilitate analyte adsorption, and recyclability.[39] In light of their attractive properties, various MOFs have been explored as sensing platforms for diverse categories of analytes.[40–44] They have also been explored in chemical sensing.[45,46] Recent research reports also document their emerging significance in fluorescence and photoelectrochemical assays.[37,38] Some recent review studies have reviewed the performance of MOF-based fluorescence sensors for different applications.[47] One of the MOFs with fluorescence characteristics, namely 4-sulfo-1,8-naphthalimide immobilized UiO-66-NH$_2$, has been used for the detection of Cr(III) (with a detection limit of 18.3 μM) and Cr(VI) (with a detection limit of 3.42 μM).[48] Likewise, a MOF doped with sulphur quantum dots (SQDs) has been proposed as a chemical sensor for Cr$_2$O$_7^{2-}$ and CrO$_4^{2-}$ ions.[47] The fluorescence of the above composite was quenched in the presence of Cr(VI) *via* the inner filter effect. A detection limit of 0.16 μM was reported.

Zinc-based MOFs are one of the most extensive ones in the category explored for sensing purposes. Some of the Zn-based MOFs exhibit light absorption from the UV to the visible spectrum and also yield significant fluorescence.[41,49] The biocompatibility along with chemical and environmental stabilities of such Zn-based MOFs underpins their potential in chemosensing applications.[50,51] Nonetheless, Zn-MOFs are not much explored as chemosensors for hazardous pollutants like Cr(VI).[52] Bio-MOF-1 is one such Zn-based MOF which is prepared with organic ligands like adenine and amino acids.[53,54] This MOF has been proposed for applications like drug delivery and gas adsorption/separation.[55]

The present work, for the first time, demonstrates the utilization of Bio-MOF-1 as a simple optical nanoprobe for Cr(VI). To achieve the said objective, we have modified Bio-MOF-1 with ascorbic acid and the resulting biocompatible and photostable Bio-MOF-1/AA nanoprobe yields highly sensitive optical (both visual and fluorescence-based) detection of Cr(VI). The introduction of AA within Bio-MOF-1 facilitates the reduction of Cr(VI) into Cr(III), thereby allowing a selective visual detection. The method is rapid and applicable in real water and food samples.

2. Experimental section

2.1. Materials

High-purity zinc acetate dihydrate (CH$_3$COO)$_2$Zn·2H$_2$O, biphenyl-4,4′-dicarboxylic acid (BPDC, C$_{14}$H$_{10}$O$_4$), and adenine (C$_5$H$_5$N$_5$) were purchased from Sigma, India. Ascorbic acid was purchased from Alfa Aesar, India. Other metal salts used in the study and the standard stock solutions (1 g L^{-1} standard for atomic absorption spectrometry) of metal ions were also purchased from Sigma, India. Deionized water (DI water, ≥18 MΩ cm^{-1}) was used throughout the experiments for the preparation of the aqueous solutions.

2.2. Characterization

Spectroscopic studies were performed using a UV-Vis spectrophotometer (Varian Cary 4000, Agilent, USA), a Fourier transform infrared spectrometer (FT-IR, Nicolet iS10, Thermo Fisher Scientific, USA), an X-ray photoelectron spectrometer (XPS) (Omicron Nanotechnology), and a photoluminescence spectrophotometer (Cary Eclipse, Agilent Technologies). X-ray diffraction patterns were collected with an X-ray diffractometer from Bruker, Germany (XRD, D8 Advance, Cu Kα = 1.54 Å, 2θ range = 5–70°, step size = 0.02°). Morphological studies were performed using scanning (SEM, SU8010, Hitachi Japan) and transmission (TEM, JEM 2100 PLUS, Jeol) electron microscopy systems. Real sample validation was performed by inductively coupled plasma-mass spectroscopy (ICP-MS, CAP RQ, Thermo Scientific).

2.3. Synthesis of Bio-MOF-1 and its functionalization with ascorbic acid (AA)

A green synthesis hydrothermal route was adopted to synthesize Bio-MOF-1. This modified approach is simpler than the previously reported solvothermal methods.[56,57] The required precursors, namely 0.05 M CH$_3$(COO)$_2$Zn·2H$_2$O (50 mL, solution 'A') and a mixture of 0.05 M adenine and 0.1 M BPDC (160 mL, solution 'B') were prepared in DI water. Solution 'A' was added dropwise to solution 'B', followed by stirring of the resulting mixture for 10 min at room temperature (RT, 25 ± 2 °C). The contents were then further reacted by refluxing for 24 h (130 °C). The obtained white crystallites were washed and then collected after filtration. The prepared Bio-MOF-1 product was dried in a vacuum oven for 24 h at 70 °C.

Next, Bio-MOF-1 was functionalized with AA using the grafting method. For this, 70 mM AA solution was mixed with a 0.5 mM aqueous suspension of Bio-MOF-1, inducing a coordination reaction between Zn^{2+} and the functional groups of ascorbic acid. The mixture was stirred and then allowed to dry in a vacuum oven at 80 °C. The above step resulted in the formation of a water-stable ascorbic acid functionalized 'Bio-MOF-1/AA' product.

2.4. Detection of Cr(VI)

2 mg of Bio-MOF-1/AA was dispersed in DI water to obtain a stock solution (2 mg mL^{-1}, pH 7.0). In all the experiments described for the sensing of the target analyte, 200 μL of the stock Bio-MOF-1/AA solution was added to different concentrations (100 μL) of Cr(VI) solutions. The final volume was always maintained at 300 μL to nullify the dilution effects. After 2 min of incubation at RT, the photoluminescence (PL) spectra were recorded at an excitation wavelength of 335 nm. The changes in the PL intensities at an emission wavelength of 460 nm were measured and correlated with the corresponding Cr(VI) concentrations. For assessment of the selectivity of the Bio-MOF-1/AA nanoprobe towards Cr(VI), its response was investigated for several other metal ions, such as 20 ng mL^{-1} of As(V), Cr(III), Fe(III), Tb(III), Eu(III), Pb(II), Hg(II), Cd(II), Co(II), Cu(II), Se(II), Mg(II), and Na(I).

2.5. Optimization of sensing parameters

The best conditions for the sensing of Cr(VI) with the Bio-MOF-1/AA nanoprobe have been identified by investigating the effect of several parameters, including the pH of the test solutions, the concentration of ascorbic acid to functionalize Bio-MOF-1, the incubation or response time to achieve a stable PL response, etc.

2.6. Analysis of Cr(VI) in some real samples

The practical utility of the Bio-MOF-1/AA nanoprobe has been established by evaluating its performance toward the analysis of Cr(VI) in samples of tap water (local sample from Chandigarh, India), lake water (Sukhna Lake, Chandigarh), and basil leaves (procured from a local market, Chandigarh, India). All these real samples were spiked with known concentrations of Cr(VI) (i.e., 6, 8, 10 ng mL^{-1}). In the case of basil leaves (Ocimum sanctum), a 200 g sample was first reacted with aqueous methanol (50 °C, 1 h). The filtrate was separated and then spiked with Cr(VI).

For quantification, 200 μL of Bio-MOF-1/AA solution was added to 100 μL of the analyte sample. These were allowed to incubate for 2 min, followed by the measurement of the PL intensity at an emission wavelength of 460 nm.

3. Results and discussion

3.1. Characterization of the Bio-MOF-1/AA nanoprobe

3.1.1. **Morphological and structural characterization.** The surface morphologies and structures of different samples were studied by scanning and transmission electron microscopy. The FE-SEM studies (Fig. 1a and b) show that Bio-MOF-1 crystallizes into a tetragonal-prism-like structure. Following its functionalization with ascorbic acid (AA), some dense and irregularly shaped spherulite can be observed over the surface of Bio-MOF-1 (Fig. 1b). The resulting Bio-MOF-1/AA structure shows a relatively rough surface morphology, which can be taken as a good indicator for the successful functionalization of Bio-MOF-1 with AA. The elemental distribution of Bio-MOF-1, as determined by EDX and mapping analysis (Fig. S1 and S2, ESI†), clearly indicates the uniform distribution of Zn, N, O, and C elements.

The TEM images and the selected area electron diffraction (SAED) patterns of Bio-MOF-1 and Bio-MOF-1/AA samples are also provided in Fig. 1(c and d). The TEM analysis again highlights a tetragonal-prism-like structure of Bio-MOF-1. The functionalization with AA is also indicated by an apparent modification in the morphology. The SAED patterns of Bio-MOF-1 and Bio-MOF-1/AA indicate toward their formation into a desired crystalline form, which is confirmed further through powder XRD analysis. The XRD pattern of Bio-MOF-1 is clearly indicative of a crystalline structure as the standard diffraction peaks are observed at 6.3°, 13.8°, and 19.8°, associated with the (111), (222), and (440) planes (Fig. 2a).[58] These results are in agreement with the previous literature, suggesting the desired phase purity of the synthesized Bio-MOF-1.[59] The XRD patterns of AA and Bio-MOF-1/AA samples are shown in Fig. 2b. AA exhibits a polycrystalline nature, as also reported in the previous literature.[60] In the XRD pattern of Bio-MOF-1/AA, all the peaks of the parent MOF, i.e., Bio-MOF-1, are retained while the characteristic peaks from AA also appear. The above XRD studies provide useful evidence about the successful functionalization of Bio-MOF-1 with AA.

3.1.2. **FTIR studies.** Fig. 2(c and d) show the FTIR spectra of Bio-MOF-1 and Bio-MOF-1/AA. In Bio-MOF-1, the strong bands at 1777 and 1627 cm^{-1} can be attributed to the carboxylic group (C=O) and C=C stretching vibrations of 4,4-biphenyl dicarboxylic acid (BPDC).[57,61] The characteristic bands of adenine (N–H stretching vibration) are found between 3193 and 3411 cm^{-1} to confirm the synthesis of Bio-MOF-1.[62] After functionalization with AA, a broad band around 3379 cm^{-1} pertains to the O–H stretching vibration. A band centered at 1784 cm^{-1} corresponds to the C=O stretching of the carbonyl groups, whereas two other bands at 1688 and 1634 cm^{-1} are attributed to the aromatic C=C/C=N/N–H bonds. After its functionalization with AA, the FTIR spectrum of Bio-MOF-1/AA retains all the characteristic bands. The binding of ascorbic acid's –OH groups to the unsaturated Zn^{2+} ions of Bio-MOF-1 results in the formation of a complex between AA and Bio-MOF-1. Hence, the crystal structure and morphology of the parent MOF are unaltered.

3.1.3. **Surface area analysis and thermal stability studies.** N_2 adsorption/desorption studies at 77 K have been performed to study the porous characteristics of Bio-MOF-1 and Bio-MOF-1/AA (Fig. 3a). Bio-MOF-1 and Bio-MOF-1-AA samples are found to possess BET surface areas of 1160 and 1076 m^2 g^{-1},
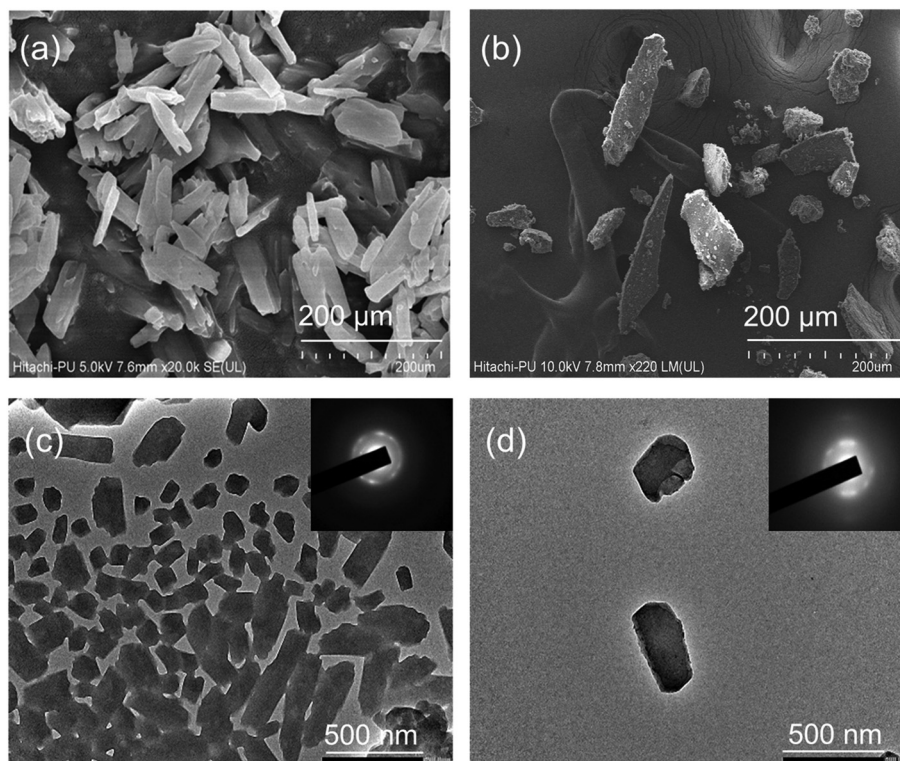
Fig. 1 Morphological characterization studies. (a) SEM image of Bio-MOF-1; (b) SEM image of Bio-MOF-1/AA; (c) TEM image and the SAED pattern of Bio-MOF-1; and (d) TEM image and the SAED pattern of Bio-MOF-1/AA.
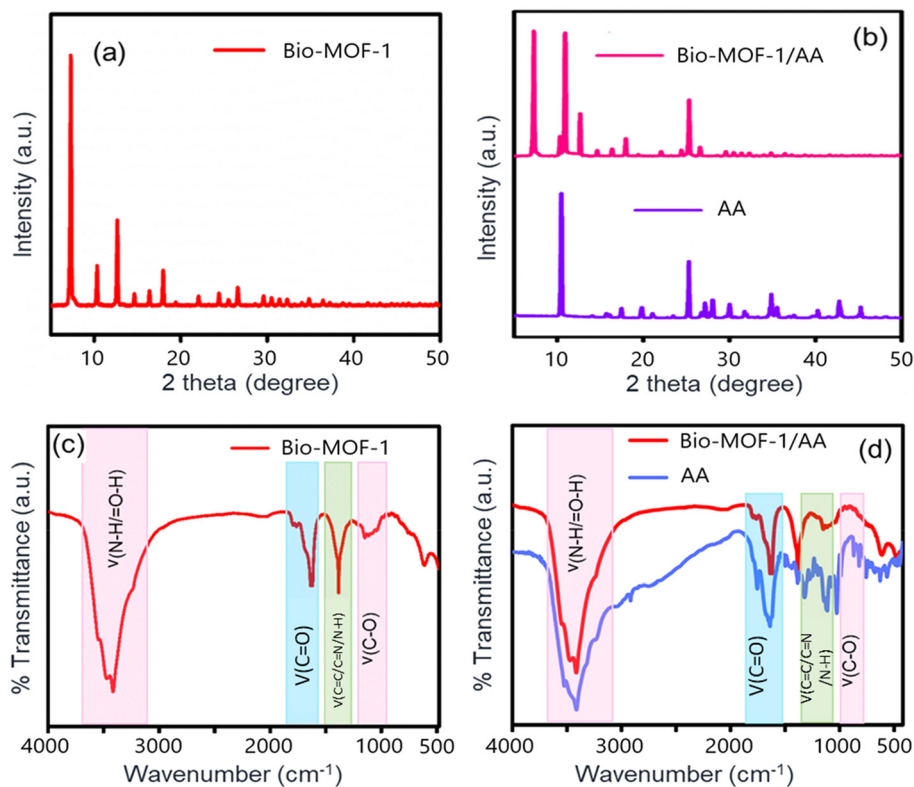

Fig. 2 XRD and FTIR characterization studies. (a) XRD of Bio-MOF-1; (b) XRD of AA and Bio-MOF-1/AA; (c) FTIR of Bio-MOF-1; and (d) FTIR of AA and Bio-MOF-1/AA.
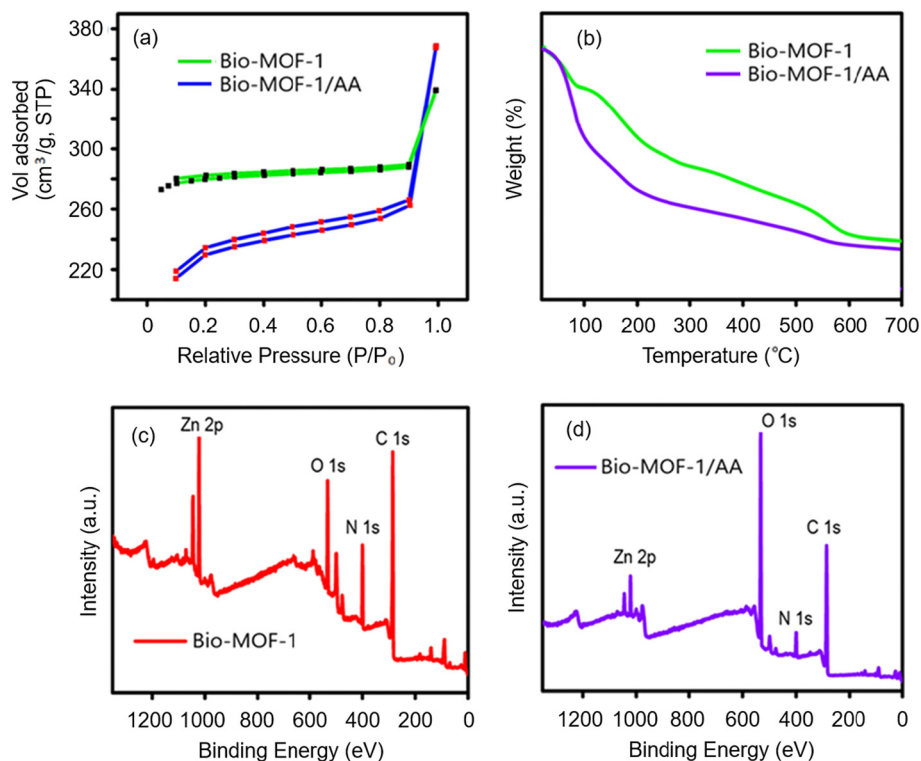
Fig. 3 Material characterization studies of the synthesized products. (a) BET surface analysis of Bio-MOF-1/AA; (b) TGA curve of Bio-MOF-1/AA; and (c and d) XPS spectra of Bio-MOF-1 and Bio-MOF-1/AA.

respectively. Their respective total pore volumes are 0.38 and 0.30 $cm^3 g^{-1}$. N_2 adsorption/desorption curves exhibit type IV isotherms, which highlight a mesoporous characteristic. The pore size distribution curves (BJH-derived estimation) reveal the pore diameters of 2.5 nm for Bio-MOF-1 and 2.4 nm for Bio-MOF-1/AA (Fig. S3†). A little reduction in the pore diameter is observed after the functionalization of Bio-MOF-1 with AA.

The thermal stabilities of Bio-MOF-1 and Bio-MOF-1/AA have also been investigated by thermogravimetric (TGA) analysis, performed under an inert N_2 atmosphere (Fig. 3b). As the results reveal, the functionalization of Bio-MOF-1 with AA causes some compromise on its thermal stability. The Bio-MOF-1/AA sample undergoes an initial weight loss of around 16%, occurring at around 200 °C. The above weight loss is because of the loss of water molecules and gaseous atoms trapped inside the pores.[63,64] A second stage loss of around 45% from 360–650 °C is associated with the release of the ligand and the degradation of the framework to form ZnO. Thus, the synthesized Bio-MOF-1/AA has good thermal stability at least up to 360 °C. The thermal stability of Bio-MOF-1/AA was further studied by XRD and FTIR studies. The samples were thermally annealed between 380 and 500 °C. The annealed samples reveal a high crystallinity, similar to the parent Bio-MOF-1 sample (Fig. S4a†).[65,66] A prolonged (*e.g.*, 24 h@380 °C) or a high temperature (*e.g.*, 500 °C for 1 h) annealing step results in the appearance of short-range peaks (high angle diffraction to suggest the formation of ZnO), indicative of a complete framework collapse. Furthermore, FTIR

studies of the annealed Bio-MOF-1/AA samples (Fig. S4b†) also highlight that the main characteristic bands are observable at least up to 400 °C. Here again, the treatment at higher temperatures causes the symmetric and asymmetric stretching IR modes of carboxylates to appear at 1680–1300 cm^{-1}. The dissociation of the structure at high temperatures is accompanied by a new broad band around 800–500 cm^{-1} from the formation of ZnO. The data collected from the different studies suggest that the functionalization of Bio-MOF-1 with AA causes some influence on its thermal stability. Nonetheless, the Bio-MOF-1/AA nanoprobe is considerably stable to implicate its potential usefulness as a nanosensor for Cr(VI).

3.1.4. X-ray photoluminescence (XPS) analysis. Bio-MOF-1 and Bio-MOF-1/AA samples have been analyzed by X-ray photoelectron spectroscopy (XPS) (Fig. 3c and d). In both samples, the spectra reveal the presence of the Zn 2p ($2p_{3/2}$) peak of ZnO_4 tetrahedral coordination at a binding energy (BE) of 1024.5 eV. Other noticeable peaks are of symmetric O 1s at a BE of 528.7 eV, N 1s at a BE of 400 eV, and C 1s at a BE of 287 eV. Fig. S5 and S6 (ESI†) show the individual spectrum of C 1s, which displays three peaks with BEs of 84.6, 286.5, and 288.2 eV, corresponding to the C–C, C=O, and –COOH functional groups, respectively.[67] As shown in Fig. S5 and S6,† the spectrum of N 1s shows a peak with a BE of 399.5 eV, associated with the existence of $-NH_2/NH_3^+$ and $-NH_2$ units.[68] The O 1s spectrum contains a characteristic peak of the bridging hydroxyl (μ^3-OH) group at a BE of 532.3 eV. Zn carboxylate peaks are observed at 531.6 and 531.4 eV.[69] Also, the emer-
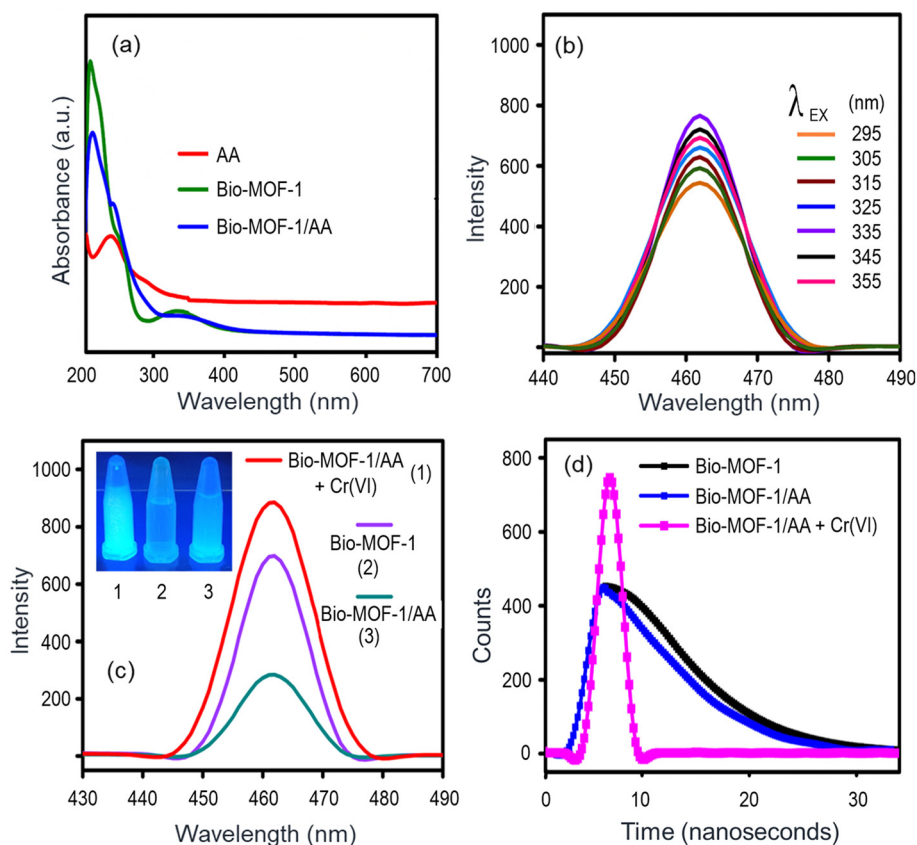
Fig. 4 Spectrophotometric properties. (a) UV-Vis spectra of Bio-MOF-1, AA, and Bio-MOF-1/AA; (b) PL spectra of Bio-MOF-1 at different excitation wavelengths; (c) PL spectra of Bio-MOF-1, Bio-MOF-1/AA, and Bio-MOF-1/AA-Cr(VI) samples; the inset shows the photograph of samples under a UV trans-illuminator; and (d) fluorescence decay curves of Bio-MOF-1, Bio-MOF-1/AA, and Bio-MOF-1/AA-Cr(VI) samples.

gence of Zn 2p peaks at 1021.6 and 1044.7 eV verify the presence of Zn.[67] Striking evidence for the formation of Bio-MOF-1/AA comes from a considerable reduction in the intensity of the Zn 2p peaks because of the coordinative binding of ascorbate moieties with unsaturated Zn^{2+} present on the external surface of Bio-MOF-1.

3.1.5. Spectroscopic properties. The UV-Vis absorption spectra of Bio-MOF-1, AA and Bio-MOF-1/AA are shown in Fig. 4a. In the case of Bio-MOF-1, a broad absorption peak (230–280 nm) originates due to the energy transfer from the organic linker (BPDC) to the Zn–O cluster. A broad peak from 300–390 nm is assigned to the $-NH_2$ groups present in adenine. After functionalization with AA, a distinct additional peak (266 nm) can be seen in the spectrum of Bio-MOF-1/AA. The photoluminescence (PL) spectra of Bio-MOF-1 under different excitation wavelengths indicate an emission maximum at 460 nm (Fig. 5b). A selection of 335 nm wavelength for excitation yields the maximum PL intensity.

3.2. Optimization of conditions for sensing of Cr(VI) with the Bio-MOF-1/AA nanoprobe

Bio-MOF-1 shows visible photoluminescence in its native form with an emission peak at 460 nm (Fig. 4b and c). Its functionalization with AA causes the quenching of the photo-

luminescence (Fig. 4c). The presence of Cr(VI) again restores the photoluminescence (the "Turn-on" mechanism) as the metal ion is reduced to Cr(III) (Fig. 4c). Therefore, it is necessary to optimize various parameters to establish the best performance conditions for the Bio-MOF-1/AA nanoprobe. The effect of the pH of the test solution on the photoluminescence (PL) intensity of Bio-MOF-1/AA is summarized in Fig. S7a.† The Bio-MOF-1/AA nanoprobe can retain its PL characteristics across a broad range of pH values (e.g., pH 3–9). A relatively high acidic condition, e.g., pH 1, could cause the protonation of the free amine groups to $-NH_3^+$ to disrupt the conjugation in the framework, consequently resulting in a reduced PL intensity. Nonetheless, the Bio-MOF-1/AA nanoprobe is useful to detect Cr(VI) samples under varying pH conditions.

The functionalization of Bio-MOF-1 with AA causes the reduction of Cr(VI) to Cr(III), which is a major governing mechanism to realize the optical detection of Cr(VI). Therefore, it becomes important to optimize the content of AA in the nanoprobe. As shown in Fig. S7b,† 70 nM AA is required to completely quench the emission from the pristine Bio-MOF-1. Hence, 70 mM AA was maintained in all the nanoprobe solutions used for the detection of Cr(VI).

The response time of the nanoprobe for the detection of Cr(VI) has also been studied. For this, the Bio-MOF-1/AA dis-
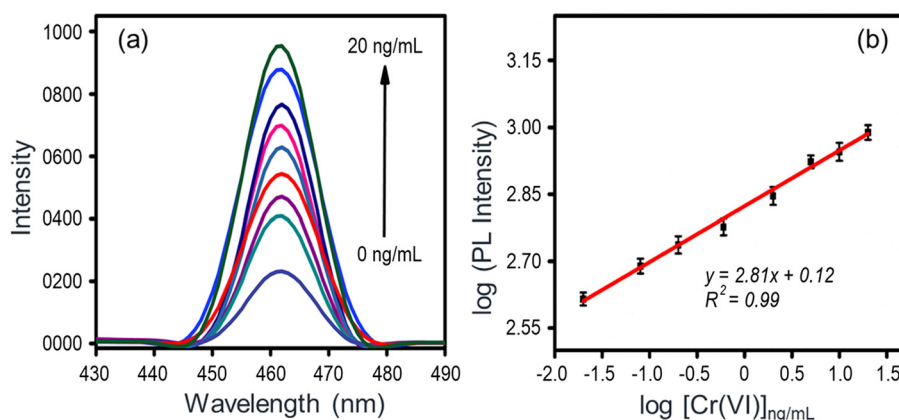
Fig. 5 Detection of Cr(VI) with the Bio-MOF-1/AA nanoprobe. (a) PL spectra in the presence of varying analyte concentrations (0.02, 0.08, 0.2, 0.6, 2, 5, 10, and 20 ng mL^{-1}) and (b) calibration plot between the PL intensity and Cr(VI) concentrations. Experimental conditions: pH = 7.0, [Bio-MOF-1/AA] = 2 mg mL^{-1}, excitation wavelength = 335 nm; error bars are based on standard deviations observed in triplicate analysis.

persion (200 μL, 2 mg mL^{-1}) was added to 100 μL of 0.001 nM Cr(VI). The color of the solution develops rapidly within the first two minutes and becomes stable thereafter (Fig. S7c,† inset). Similarly, the PL intensity of the solution increases and saturates within 2 min (Fig. S7†). Thus, the Bio-MOF-1/AA nanoprobe should allow rapid testing of Cr(VI) in aqueous solutions.

3.3. Detection of Cr(VI) with the Bio-MOF-1/AA nanoprobe

As shown in Fig. 4c, the functionalization of Bio-MOF-1 with AA causes the emission to quench. An overlap between the absorption bands of Bio-MOF-1 and AA (Fig. 4a) can be expressed as a reason for the above-observed quenching.[70,71] The addition of Cr(VI) solutions (0.02–20 ng mL^{-1}) to the Bio-MOF-1/AA nanoprobe leads to a proportional recovery of the PL, as shown in Fig. 5a. This detection of Cr(VI) is also visibly perceived as a colorless nanoprobe solution turns ice blue and then becomes intense with the increasing concentration of the metal ion (Fig. S8†).

As the results (Fig. 5a) highlight, the PL properties of Bio-MOF-1/AA are extremely sensitive towards Cr(VI). A calibration curve (log-scale) between the PL intensity and the analyte concentration is shown in Fig. 5b where a correlation coefficient (R^2) of 0.99 suggests a good linear fitting of the data. Based on the standard protocol ($3\sigma/m$, σ = standard deviation of the blank solution and m = slope of the calibration curve),[44] the limit of detection (LOD) is estimated to be 0.01 ng mL^{-1}, which is much lower than the maximum permissible level of Cr(VI) in drinking water as recommended by the WHO (0.05 mg L^{-1}).[7]

Table S1† summarizes the sensing performances of the different fluorescence probes reported recently for Cr(VI) detection.[28,29,72–77] Compared to most of those methods, the present nanoprobe offers a lower limit of detection. The detection is achieved over a fairly wide concentration range, *i.e.*, 20 pg mL^{-1} to 20 ng mL^{-1}. The response time of the sensor is also quick. Hence, this work contributes to the realization of a

new platform for the simultaneous colorimetric and fluorescence detection of Cr(VI) ions.

3.4. Selectivity, reproducibility, and stability studies

The selectivity of the Bio-MOF-1/AA nanoprobe for Cr(VI) has been evaluated against different potentially co-existing cations, such as As(V), Cr(III), Fe(III), Tb(III), Eu(III), Pb(II), Hg(II), Cd(II), Co(II), Cu(II), Se(II), Mg(II), and Na(I). The experimental conditions and results are depicted in Fig. 6a. Clearly, the PL of the Bio-MOF-1/AA nanoprobe remains unchanged upon addition of the abovementioned potential interferents even in high concentrations. The nanoprobe yields a selective response to Cr(VI) even in a complex solution mixture containing Cr(VI) and many other cations.

The reproducibility of the Bio-MOF-1/AA nanoprobe has been investigated. For this, five different nanoprobe solutions were prepared and tested to analyze a fixed concentration (10 ng mL^{-1} Cr(VI)), maintaining similar experimental conditions. Fig. 6b shows the results in terms of PL recovery. The data reveal a high degree of reproducibility in the sensor response with the coefficient of variance not exceeding 4.4%. The experimental data from the above reproducibility study were further analysed by one-way 'Analysis of Variance' (ANOVA) along with Tukey's Honestly Significant Difference (HSD) *post hoc* test to determine their statistical significance. Such statistical approaches to sensor systems have been recommended in earlier literature also.[78,79] As listed in Table S2,† the obtained *p*-value of 2.1294×10^{-13}, attributed to the *F*-statistic of one-way ANOVA, is less than 0.05, suggesting that the results are statistically significant. Additionally, Tukey's *t*-test was applied to all the possible matching pairs of the experimental samples from different cycles. As shown in Table S3,† significant differences ($p < 0.01$), consistently for each pair, again indicate that the obtained results are statistically significant.

The shelf-life or stability of the Bio-MOF-1/AA nanoprobe was tested for a span of 30 days (storage at 4 °C). The nanoprobe solution was periodically used to test its response for 10
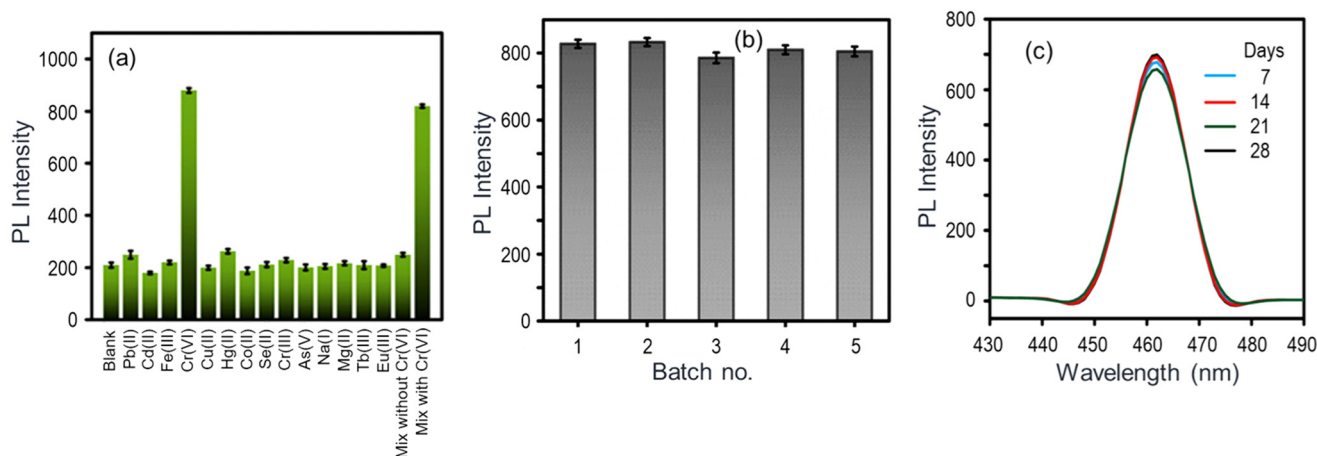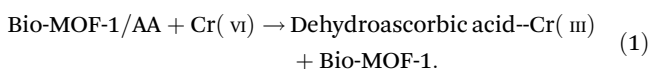
Fig. 6 Assessment of different important quality assurance aspects of the Bio-MOF-1/AA nanoprobe. (a) Sensor response in terms of PL enhancement toward Cr(vi) and various other potentially co-existing metal ions; (b) PL response of five different nanoprobe solutions against 10 ng mL^{-1} Cr (vi); and (c) PL spectra of the nanoprobe solution stored for 4 weeks.

ng mL^{-1} Cr(vi) solution. The Bio-MOF-1/AA nanoprobe significantly retains its original fluorescence intensity (PL reduction of <5%) for at least up to 4 weeks (Fig. 6c). As the above studies revealed, the Bio-MOF-1/AA nanoprobe performs well on different key quality assurance aspects of a nanosensor.

3.4.1. Mechanism of the detection process

3.4.1.1. Quenching. The functionalization of Bio-MOF-1 with ascorbic acid (AA) causes the fluorescence to quench. This can be explained by the light absorption characteristics of Bio-MOF-1 and AA (Fig. 4a) wherein both of their absorption bands overlap. It results in a competitive absorption of the excitation energy and subsequently the emission from Bio-MOF-1 is reduced. The fluorescence decay lifetime experiments (excitation wavelength = 335 nm, emission wavelength = 460 nm) also reveal a reduction in the lifetime of Bio-MOF-1 from 2.52 to 2.36 ns, suggesting a kinetic quenching process (Fig. 4d).

3.4.1.2. Fluorescence recovery. The addition of Cr(vi) to the Bio-MOF-1/AA probe is associated with the recovery of fluorescence. AA forms a complex with Cr(vi) *via* the oxygen containing groups. A rapid electron transfer process takes place to produce dehydroascorbic acid (DHA) and Cr(iii) as the final reaction products. In this process, AA is dissociated from the structure of Bio-MOF-1 to form an ascorbate complex (eqn (1)). Since Bio-MOF-1 recovers to its unfunctionalized form, it shows an increase (or recovery) of emission characteristics. Apart from the PL signal, a visual change in the color of the nanoprobe solution is also seen (Fig. S8†).

$$\begin{aligned} \text{Bio-MOF-1/AA} + \text{Cr(vi)} &\rightarrow \text{Dehydroascorbic acid--Cr(iii)} \\ &+ \text{Bio-MOF-1}. \end{aligned} \quad (1)$$

The morphological (SEM) analysis of the reaction product (refer to eqn (1)) after a detection experiment indicates the presence of both regular (Bio-MOF-1) and agglomerated irregular (dehydroascorbic acid–Cr(iii)) structures (Fig. S9a†). The

(dehydroascorbic acid–Cr(iii)) structures have relatively uneven and rough morphologies. The EDS mapping of the reaction products has also revealed the presence of C, O, Zn, and Cr confirming the adsorption of Cr(vi) (Fig. S9b and c†). The relative amount of O increases from 23% to 41% while the O/C ratio jumps from 34% to 55%. These observations indicate the oxidation of AA alongside the reduction of Cr(vi) to Cr(iii). Therefore, the EDS data present useful evidence to confirm the capture of Cr(vi) by the Bio-MOF-1/AA probe, as expressed in eqn (1).

The reaction products were further characterized by XPS, XRD, and FTIR studies (Fig. S9d–f†). The information about the oxidation states of elements is provided by the XPS data. The reaction product shows the presence of a Cr 2p peak along with Zn 2p, O 1s, N 1s, and C 1s (Fig. S9d†). The XPS analysis of the reaction product also highlights a significant increase in the oxygen containing groups, while the intensity of the carbon peak decreases. This point reconfirms the oxidation and reduction of AA and Cr(vi), respectively. The high-resolution XPS spectra are shown in Fig. S10.† The peaks at binding energies of 577.4 eV and 586.9 eV are attributed to Cr(iii) 2p$_{3/2}$ and 2p$_{1/2}$, respectively. No other peak is observed to refer to the presence of Cr(vi), verifying that after the sensing experiment, Cr is present only as Cr(iii) on the surface of Bio-MOF-1.[80] These results further support the claim that the interaction of Cr(vi) with the Bio-MOF-1/AA probe leads to its reduction to a less toxic Cr(iii) form.

The XRD pattern of the reaction product 'DHA + Cr(iii) + Bio-MOF-1' (DHA = dehydroascorbic acid) reveals not only the diffraction peaks from a typical Bio-MOF-1 structure but also some additional peaks, suggesting the presence of a chromium–ascorbate complex (Fig. S9e†). The formation of DHA–Cr(iii) + Bio-MOF-1 is also supported by FTIR analysis (Fig. S9f†). The carbonyl stretching (C=O) in Bio-MOF-1/AA is reflected by a band at 1754 cm^{-1} which shifts to 1727 cm^{-1} in the reaction product sample. Similarly, the $\nu_{C=C}$ and $\nu_{C=O}$

bands at 1664 and 1645 cm^{-1} are shifted to 1632 cm^{-1}. The C–OH and C–O stretching (1207 cm^{-1}) disappears after the reaction due to the loss of the hydroxyl groups in the process. The above observations indicate that Cr(VI) oxidizes the hydroxyl groups of AA to generate a chromate ester intermediate, followed by the formation of a Cr(III)–ascorbate complex (eqn (1)). The presence of carbonyl groups on AA facilitates binding sites for Cr(III) ions and subsequently results in the reduction of Cr(VI) to Cr(III) as explained above.

3.5. Application of the Bio-MOF-1/AA nanoprobe to quantify Cr(VI) in real samples and validation with the ICP-MS technique

The practical utility of the Bio-MOF-1/AA nanoprobe for the sensing of Cr(VI) in real samples has been assessed by extending the studies in spiked samples of tap/lake water and the extract of basil leaves (Table S4†). In these studies, similar to the steps undertaken with synthetic samples (Section 3.2), 200 μL of Bio-MOF-1/AA solution was added to 100 μL of the test sample, and the PL spectra were recorded after 2 min. The metal ion concentrations were also quantified by ICP-MS for validation. In all the experiments, the use of the Bio-MOF-1/AA nanoprobe yielded concentration values that closely match (98–110%) with the standard ICP-MS results. Based on these findings, it can be concluded that the Bio-MOF-1/AA nanoprobe allows accurate and sensitive detection of Cr(VI) ions both in synthetic and spiked real samples.

3.6. Adsorption of Cr(VI) with Bio-MOF-1/AA

A selective response of Bio-MOF-1/AA toward Cr(VI) should allow this composite to be used as an adsorbent for water purification purposes. The pH dependence (pH: 3–11) of the adsorption capacity of Bio-MOF-1/AA (1 mg mL^{-1}) for Cr(VI) (1 μg mL^{-1}) is shown in Fig. S11.† The Bio-MOF-1/AA composite can facilitate an efficient and rapid (within 5 min) removal of around 80% of Cr(VI) from pH 3–7 in one cycle. Thus, Bio-MOF-1/AA can be further explored also for the adsorptive removal of Cr(VI) under both acidic and neutral conditions. This should attract environmental remediation applications, such as the treatment of Cr(VI) contaminated acidic wastewater effluents.

4. Conclusion

The present study has outlined the usefulness of a simple zinc-adeninate based bio-MOF as a facile, sensitive, and selective nanosensor for an important heavy metal ion, i.e., Cr(VI). A green synthesis route has been adopted to synthesize and functionalize (with ascorbic acid) the biocompatible and luminescent nanoprobe. The nanoprobe, termed "Bio-MOF-1/AA", exhibits several favourable material characteristics such as a porous structure, good thermal stability, stable luminescence, aqueous dispersibility, and cost-effectiveness. The quenched photoluminescent state of Bio-MOF-1/AA allows a "Turn-on" type of sensor response when it comes in contact with Cr(VI)

solutions. The presence of Cr(VI) is detectable both by the naked eye (generation of an ice-blue colour) and spectrophotometrically. The developed chemosensor offers a rapid (2 min) fluoro-chromic detection of Cr(VI) with a very low limit of detection, e.g., 10 pg mL^{-1}. As the Bio-MOF-1/AA nanoprobe is demonstrated to be equally efficient to detect Cr(VI) in some spiked real samples, it speaks about the practical utility of the presented method. Owing to its simplicity, sensitivity, low-cost, and portability, the Bio-MOF-1/AA nanoprobe can be projected as a viable option with broad applications in environmental and food quality monitoring. In the future, this nanoprobe can also be integrated with a microfluidic device or dip-stick assays to allow rapid and user-friendly on-site detection of heavy metals in different environmental samples.

Author contributions

Gurjeet Kaur: visualization, experimental work, writing – original draft, data interpretation, formal analysis, validation, and conceptualization; Saloni Sharma: data curation, software, formal analysis, and validation; Manoj K. Nayak: writing – review and editing, supervision, conceptualization, and resources; Akash Deep: project administration, writing – review and editing, supervision, conceptualization, resources, and funding acquisition.

Conflicts of interest

There are no conflicts to declare.

Acknowledgements

References

1 R. Sreekanth, V. Pattabhi and S. Rajan, *Biochem. Biophys. Res. Commun.*, 2008, **369**, 725–729.

2 S. Comber and M. Gardner, *J. Environ. Monit.*, 2003, **5**, 410–413.

3 M.-N. Georgaki, M. Charalambous, N. Kazakis, M. A. Talias, C. Georgakis, T. Papamitsou and C. Mytiglaki, *Environments*, 2023, **10**, 33.

4 S. Sadeghi and A. Z. Moghaddam, *J. Iran. Chem. Soc.*, 2016, **13**, 117–130.

5 H. G. Preuss, B. Echard, N. V. Perricone, D. Bagchi, T. Yasmin and S. J. Stohs, *J. Inorg. Biochem.*, 2008, **102**, 1986–1990.

6 A. S. K. Kumar, S.-J. Jiang and W.-L. Tseng, *J. Mater. Chem. A*, 2015, **3**, 7044–7057.

7 J. Wei, Z. Guo, X. Chen, D.-D. Han, X.-K. Wang and X.-J. Huang, *Anal. Chem.*, 2015, **87**, 1991–1998.

8 A. Zhitkovich, *Chem. Res. Toxicol.*, 2005, **1**, 3–11.

9 Z. Wang and C. Yang, *Advances in Pharmacology*, Elsevier, 2023, vol. 96, pp. 241–265.

10 M. Cieślak-Golonka, *Polyhedron*, 1996, **15**, 3667–3689.

11 U.S. Department of Health and Human Services, *Managing hazardous materials incidents: medical management guidelines for acute chemical exposures*, 2001, vol. **3**.

12 S. Tiwari, M. K. Deb and B. K. Sen, *Food Chem.*, 2017, **221**, 47–53.

13 Y.-T. Zhuang, S. Chen, R. Jiang, Y.-L. Yu and J.-H. Wang, *Anal. Chem.*, 2019, **91**, 5346–5353.

14 A. Kazemi, M. Esmaeilbeigi, Z. Sahebi and A. Ansari, *Sci. Total Environ.*, 2022, **807**, 150795.

15 P. Liang, Q. Ding and Y. Liu, *J. Sep. Sci.*, 2006, **29**, 242–247.

16 G. Rahman, H. Kingston, T. G. Towns, R. J. Vitale and K. R. Clay, *Anal. Bioanal. Chem.*, 2005, **382**, 1111–1120.

17 K. Kiran, K. S. Kumar, B. Prasad, K. Suvardhan, R. B. Lekkala and K. Janardhanam, *J. Hazard. Mater.*, 2008, **150**, 582–586.

18 M. Safari, S. Nojavan, S. S. H. Davarani and A. Morteza-Najarian, *Anal. Chim. Acta*, 2013, **789**, 58–64.

19 Z. Qiu, D. Tang, J. Shu, G. Chen and D. Tang, *Biosens. Bioelectron.*, 2016, **75**, 108–115.

20 L. Lu, X. Han, J. Lin, Y. Zhang, M. Qiu, Y. Chen, M. Li and D. Tang, *Analyst*, 2021, **146**, 2664–2669.

21 R. Kanagaraj, Y.-S. Nam, S. J. Pai, S. S. Han and K.-B. Lee, *Sens. Actuators, B*, 2017, **251**, 683–691.

22 F. Tan, L. Cong, X. Jiang, Y. Wang, X. Quan, J. Chen and A. Mulchandani, *Sens. Actuators, B*, 2017, **247**, 265–272.

23 S. Bothra, R. Kumar and S. K. Sahoo, *New J. Chem.*, 2017, **41**, 7339–7346.

24 S. Rapti, D. Sarma, S. A. Diamantis, E. Skliri, G. S. Armatas, A. C. Tsipis, Y. S. Hassan, M. Alkordi, C. D. Malliakas and M. G. Kanatzidis, *J. Mater. Chem. A*, 2017, **5**, 14707–14719.

25 C. Mendoza, G. Cortes and D. Munoz, *Environ. Toxicol. Water Qual.*, 1996, **11**, 327–333.

26 H. Sharma, N. Kaur, A. Singh, A. Kuwar and N. Singh, *J. Mater. Chem. C*, 2016, **4**, 5154–5194.

27 H. Jiang, W. Zhang, P. Chen, W. Zhang, G. Wang, X. Luo and S. Luo, *J. Mater. Chem. A*, 2016, **4**, 11897–11907.

28 J. Duan, L. Zhao, W. Lv, Y. Li, Y. Zhang, S. Ai and L. Zhu, *Microchem. J.*, 2019, **150**, 104105.

29 S. Ebrahim, A. Shokry, M. Khalil, H. Ibrahim and M. Soliman, *Sci. Rep.*, 2020, **10**, 13617.

30 A. Bilgiç and A. Çimen, *J. Mol. Liq.*, 2020, **312**, 113398.

31 Y. Liu, J. Li, D. Yin, Y. Liu, L. Wang, Z. Zhang, R. Zheng and Y. Huang, *Tetrahedron*, 2024, **150**, 133749.

32 M. Kaur, M. Yusuf and A. K. Malik, *J. Fluoresc.*, 2023, **33**, 61–75.

33 X. Wang, Y. Zuo, Y. Zhang, T. Yang and W. Lin, *Analyst*, 2019, **144**, 5373–5377.

34 Z. Li, C. Li and H. Yan, *RSC Adv.*, 2021, **11**, 8963–8969.

35 Z. Qiu, D. Tang, J. Shu, G. Chen and D. Tang, *Biosens. Bioelectron.*, 2016, **75**, 108–115.

36 N. A. Nordin, M. A. Mohamed, M. N. I. Salehmin and S. F. M. Yusoff, *Coord. Chem. Rev.*, 2022, **468**, 214639.

37 S. Lv, Y. Tang, K. Zhang and D. Tang, *Anal. Chem.*, 2018, **90**, 14121–14125.

38 Y. Gao, M. Li, Y. Zeng, X. Liu and D. Tang, *Anal. Chem.*, 2022, **94**, 13582–13589.

39 N. Xia, Y. Chang, Q. Zhou, S. Ding and F. Gao, *Biosensors*, 2022, **12**, 928.

40 Y. Liu, X.-Y. Xie, C. Cheng, Z.-S. Shao and H.-S. Wang, *J. Mater. Chem. C*, 2019, **7**, 10743–10763.

41 L. Shi, N. Li, D. Wang, M. Fan, S. Zhang and Z. Gong, *TrAC, Trends Anal. Chem.*, 2021, **134**, 116131.

42 D. Kukkar, K. Vellingiri, K.-H. Kim and A. Deep, *Sens. Actuators, B*, 2018, **273**, 1346–1370.

43 G. Kaur, S. Sharma, S. Singh, N. Bhardwaj and A. Deep, *ACS Omega*, 2022, **7**, 17600–17608.

44 S. Sharma, G. Kaur, M. K. Nayak and A. Deep, *Environ. Sci.: Nano*, 2023, **10**, 2473–2488.

45 B. Yan, *J. Mater. Chem. C*, 2019, **7**, 8155–8175.

46 S. A. Diamantis, A. Margariti, A. D. Pournara, G. S. Papaefstathiou, M. J. Manos and T. Lazarides, *Inorg. Chem. Front.*, 2018, **5**, 1493–1511.

47 Y. Zhang, J. Liu, X. Wu, W. Tao and Z. Li, *Anal. Chim. Acta*, 2020, **1131**, 68–79.

48 A. Yildirim, M. B. Kocer, A. Uysal and M. Yilmaz, *Mater. Today Commun.*, 2022, **32**, 104117.

49 S. Gai, J. Zhang, R. Fan, K. Xing, W. Chen, K. Zhu, X. Zheng, P. Wang, X. Fang and Y. Yang, *ACS Appl. Mater. Interfaces*, 2020, **12**, 8650–8662.

50 S. C. Pal, D. Mukherjee and M. C. Das, *Inorg. Chem.*, 2022, **61**, 12396–12405.

51 W. Xie, Y. Yuan, T.-Y. Zhou, J.-J. Wang, Z.-B. Nie, Y.-H. Xu and Z.-M. Su, *J. Solid State Chem.*, 2022, **310**, 123093.

52 Z. Zhang, Y. Lou, C. Guo, Q. Jia, Y. Song, J.-Y. Tian, S. Zhang, M. Wang, L. He and M. Du, *Trends Food Sci. Technol.*, 2021, **118**, 569–588.

53 W. Chen, Y. Zhuang, L. Wang, Y. Lv, J. Liu, T.-L. Zhou and R.-J. Xie, *ACS Appl. Mater. Interfaces*, 2018, **10**, 18910–18917.

54 E. A. Giles-Mazón, I. Germán-Ramos, F. Romero-Romero, E. Reinheimer, R. A. Toscano, N. Lopez, C. E. Barrera-Díaz, V. Varela-Guerrero and M. F. Ballesteros-Rivas, *Inorg. Chim. Acta*, 2018, **469**, 306–311.

55 E. Binaeian, H. Nabipour, S. A. Nasrabadi and S. Rohani, *J. Mater. Chem. B*, 2023, 11426–11459.

56 J. Yu, Y. Cui, H. Xu, Y. Yang, Z. Wang, B. Chen and G. Qian, *Nat. Commun.*, 2013, **4**, 1–7.

57 J. An, S. J. Geib and N. L. Rosi, *J. Am. Chem. Soc.*, 2009, **131**, 8376–8377.

58 J. An, O. K. Farha, J. T. Hupp, E. Pohl, J. I. Yeh and N. L. Rosi, *Nat. Commun.*, 2012, **3**, 604.

59 D. Duan, J. Ye, X. Cai and K. Li, *Microchim. Acta*, 2021, **188**, 1–10.

60 H. M. Palma-Rodríguez, J. Alvarez-Ramírez and A. Vargas-Torres, *Starch/Stärke*, 2018, **70**, 1700323.

61 W. Liu, S.-Q. Li, J. Shao and J.-L. Tian, *J. Solid State Chem.*, 2020, **290**, 121580.

62 Q. Qian, A. X. Wu, W. S. Chi, P. A. Asinger, S. Lin, A. Hypsher and Z. P. Smith, *ACS Appl. Mater. Interfaces*, 2019, **11**, 31257–31269.

63 K. E. Diab, E. Salama, H. S. Hassan, A. Abd El-moneim and M. F. Elkady, *Sci. Rep.*, 2021, **11**, 6619.

64 H. Shokry, M. Elkady and E. Salama, *Sci. Rep.*, 2020, **10**, 10265.

65 S. J. Yang, T. Kim, J. H. Im, Y. S. Kim, K. Lee, H. Jung and C. R. Park, *Chem. Mater.*, 2012, **24**, 464–470.

66 S. Gadipelli and Z. Guo, *Chem. Mater.*, 2014, **26**, 6333–6338.

67 Y. Rachuri, J. F. Kurisingal, R. K. Chitumalla, S. Vuppala, Y. Gu, J. Jang, Y. Choe, E. Suresh and D.-W. Park, *Inorg. Chem.*, 2019, **58**, 11389–11403.

68 N. Graf, E. Yegen, T. Gross, A. Lippitz, W. Weigel, S. Krakert, A. Terfort and W. E. Unger, *Surf. Sci.*, 2009, **603**, 2849–2860.

69 Y. Wang, L. Li, P. Dai, L. Yan, L. Cao, X. Gu and X. Zhao, *J. Mater. Chem. A*, 2017, **5**, 22372–22379.

70 Y. Wang, L. Xiong, F. Geng, F. Zhang and M. Xu, *Analyst*, 2011, **136**, 4809–4814.

71 C. Yu, Y. Wu, F. Zeng and S. Wu, *J. Mater. Chem. B*, 2013, **1**, 4152–4159.

72 J. Xu, Q. Gao and Z. Wang, *ACS Appl. Nano Mater.*, 2022, **6**, 750–758.

73 Y. Liu, L. Huang, S. Mahmud and H. Liu, *J. Cluster Sci.*, 2020, **31**, 549–560.

74 Y. Jia, S. Wu, Z. Duan, S. Song, S. Shuang, X. Gong and C. Dong, *Spectrochim. Acta, Part A*, 2022, **278**, 121343.

75 A. A. Wani, A. M. Khan, Y. K. Manea, M. A. Salem and M. Shahadat, *J. Hazard. Mater.*, 2021, **416**, 125754.

76 Y. Ma, Y. Chen, J. Liu, Y. Han, S. Ma and X. Chen, *Talanta*, 2018, **185**, 249–257.

77 M. Elavarasi, S. A. Alex, N. Chandrasekaran and A. Mukherjee, *Anal. Methods*, 2014, **6**, 9554–9560.

78 L. Lu, R. Zeng, Q. Lin, X. Huang and D. Tang, *Anal. Chem.*, 2023, **95**, 16335–16342.

79 Y. Gao, Z. Yu, L. Huang, Y. Zeng, X. Liu and D. Tang, *Anal. Chem.*, 2023, **95**, 9130–9137.

80 Y. Chen, D. An, S. Sun, J. Gao and L. Qian, *Materials*, 2018, **11**, 269.